Applied Catalysis B: Environmental 202 (2017) 550–556

Contents lists available at ScienceDirect

Applied Catalysis B: Environmental

journal homepage: www.elsevier.com/locate/apcatb

Iron-embedded nitrogen doped carbon frameworks as robust catalyst for oxygen reduction reaction in microbial fuel cells

Haolin Tang[a,*], Yan Zeng[a], Yinxiang Zeng[b], Rui Wang[a], Shichang Cai[a], Cong Liao[a], Haopeng Cai[a], Xihong Lu[b,*], Panagiotis Tsiakaras[c,*]

[a] State Key Laboratory of Advanced Technology for Materials Synthesis and Processing, Wuhan University of Technology, Wuhan 430070, PR China
[b] MOE of the Key Laboratory of Bioinorganic and Synthetic Chemistry, KLGHEI of Environment and Energy Chemistry, School of Chemistry and Chemical Engineering, Sun Yat-Sen University, Guangzhou 510275, PR China
[c] Laboratory of Alternative Energy Conversion Systems, Department of Mechanical Engineering, School of Engineering, University of Thessaly, 38334 Volos, Greece

ARTICLE INFO

Article history:
Received 12 June 2016
Received in revised form
24 September 2016
Accepted 26 September 2016
Available online 28 September 2016

Keywords:
Iron-embedded nitrogen doped carbon
Microbial fuel cells
Oxygen reduction reaction
Ferroporphyrin
3D Fe-N-C framework

ABSTRACT

A kind of 3D Fe-embedded N doped carbon framework catalyst is successfully developed and tested in the present work as a robust cathode catalyst for microbial fuel cells (MFCs). Due to the well-arranged mesopores, the high surface area, the interconnected conductive networks as well as the finely dispersed Fe-N active species, the as-prepared 3D Fe-N-C catalyst exhibits significantly enhanced ORR activity compared to commercial Pt/C. More precisely, the 3D Fe-N-C yields a more-positive half-wave potential of −0.08 V (vs. SCE) and remarkably stable limiting current of ~6.2 mA cm^{-2}. The 3D Fe-N-C shows also an excellent tolerance to methanol as well as remarkably long-term stability with more than 82.4% retention of its initial activity after 55.5 h operation. Based on the as-prepared 3D Fe-N-C as the air cathode catalyst, a stable microbial fuel cell (MFC) device is fabricated and tested, performing a maximum power density of 3118.9 mW m^{-2} at a high current density of 9980.8 mA m^{-2}. More importantly, it is found that the Fe-N-C MAFC device could steadily operate for more than 250 h in a feed period, which is substantially longer than the Pt/C-MFC device.

1. Introduction

With the continuous growth of the global population and economy, there is an ever-increasing demand for renewable energy and clean water. Microbial fuel cells (MFCs) are emerging as one of the most promising systems to generate current from organic matter, which hold great promise in energy recovery from waste water, marine sediment, biomass, etc. [1–3]. Although a significant progress has been made the last years, concerning the development of MFCs, there are still many challenges such as the technical issues associated with the performance and stability that should be overcome for their practical applications [4]. A MFC device, is typically composed of an anode, on which the organic matter is oxidized by microorganisms, and a cathode that consumes the electrons derived generally by an oxidant.

Oxygen is the most favourable electron acceptor for its sustainability and widely used as air cathode in MFCs [5]. Due to the sluggish nature of oxygen reduction reaction (ORR), catalyst materials are inevitably employed in air cathode. Platinum (Pt) and Pt-based materials are well-known ORR catalysts for their high activity and desired four-electron transfer reaction during ORR process. However, Pt is very expensive, scarce and easy of poisoning that severely hinders its widespread use as air cathode catalyst in MFCs [6–8]. Thus, the development of cost-effective, efficient and stable alternatives to Pt-based catalysts for ORR is the prerequisite for practical applications of MFCs.

Currently, doping carbon materials with non-metal elements have been extensively studied as state-of-the-art catalysts for ORR in MFCs, mostly because of their promising electrocatalytic activity, low cost, environmental friendliness, and good durability [9–14]. Various non-metal heteroatoms including N [15–18], S [19–23], and P [24,25] were extensively used as dopants, demonstrating improved ORR properties. Nevertheless, their ORR activity is still inferior to that of conventional Pt/C catalysts, especially in neutral media, making them less competitive for use in MFCs. To address this issue, some transition metal species have been inten-

* Corresponding authors.
E-mail addresses: thln@whut.edu.cn (H. Tang), luxh6@mail.sysu.edu.cn (X. Lu), tsiak@uth.gr (P. Tsiakaras).

http://dx.doi.org/10.1016/j.apcatb.2016.09.062
0926-3373/

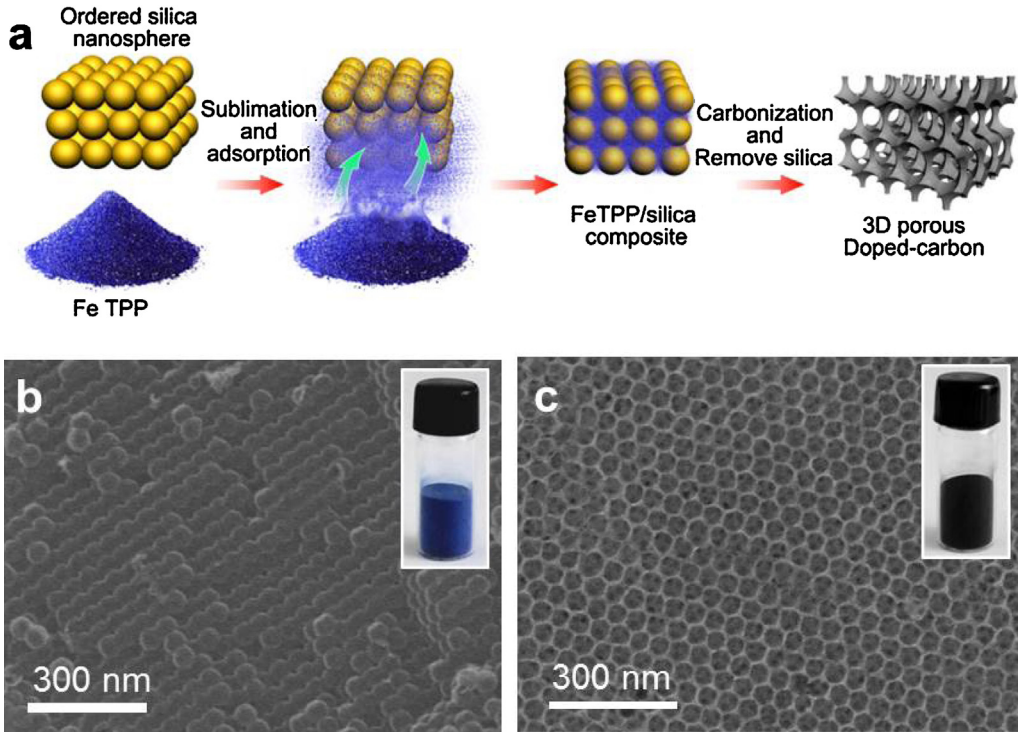

Fig. 1. (a) Schematic process for the synthesis of 3D porous Fe-N-C frameworks. SEM images of the as-prepared (b) silica spheres and (c) 3D Fe-N-C frameworks. Insets are their corresponding photo images.

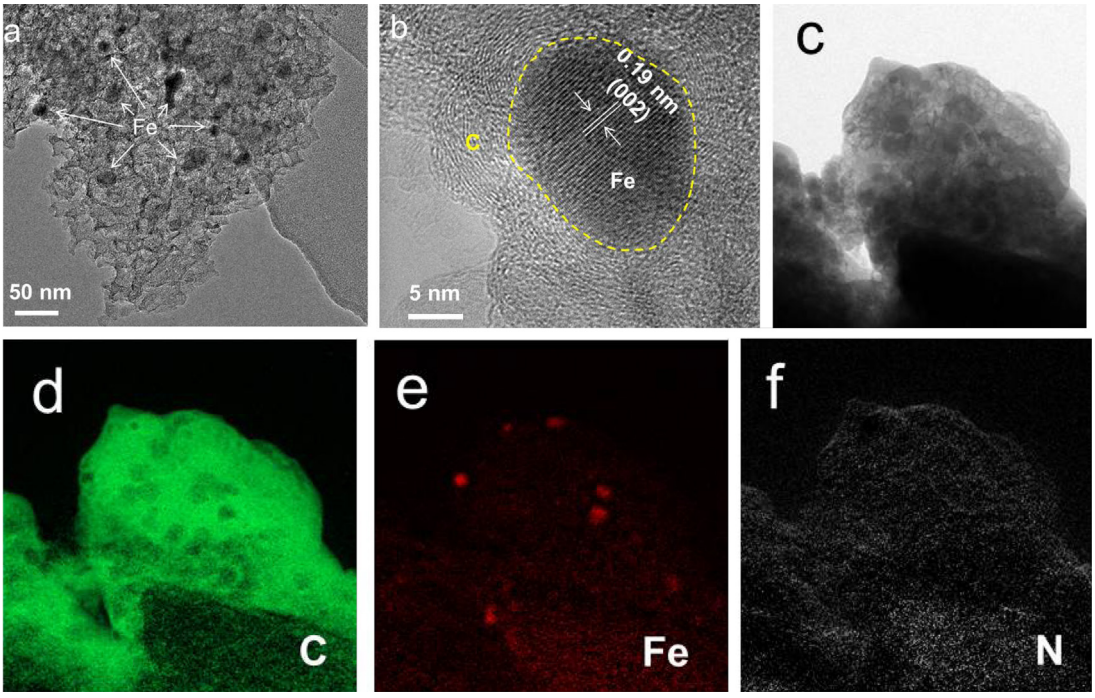

Fig. 2. (a) TEM, and (b) HRTEM images of the as-synthesized 3D Fe-N-C catalyst. (c) HAADF-STEM images of the as-synthesized 3D Fe-N-C catalyst. EELS elemental maps of (d) carbon, (e) Fe, and (f) N.

tionally introduced into these doped carbon materials to further enhance their ORR activity. This has proven to be a very promising and effective strategy although its detailed mechanism is not clearly understood yet [26–30]. For instance, core-shell structured N-Fe/Fe_3C@C has been developed and exhibited significantly improved ORR performance in neutral phosphate buffer solution (PBS) compared with the commercial Pt/C catalysts [30].

Recently, iron and nitrogen co-doped graphene catalysts have been developed using thermal treatment of a mixture of $FeCl_3$, graphitic carbon nitride, and chemically reduced graphene. The enhanced ORR activity in neutral solution provides great potential as air cathodic catalyst in MFCs [31]. However, these metal-nitrogen co-doped carbon catalysts usually suffer from the unequal distribution of active sites, less-controlled agglomeration and/or

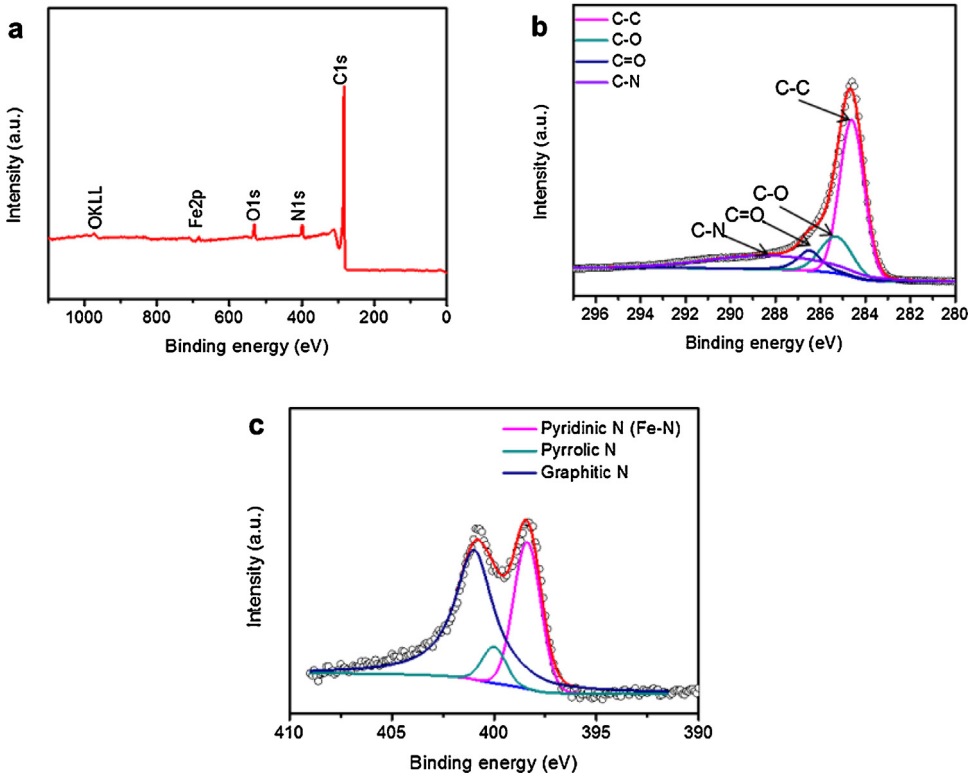

Fig. 3. (a) XPS survey, (b) Core level C1 1s and (c) Core level N 1s spectrum of the as-synthesized of 3D Fe-N-C catalyst.

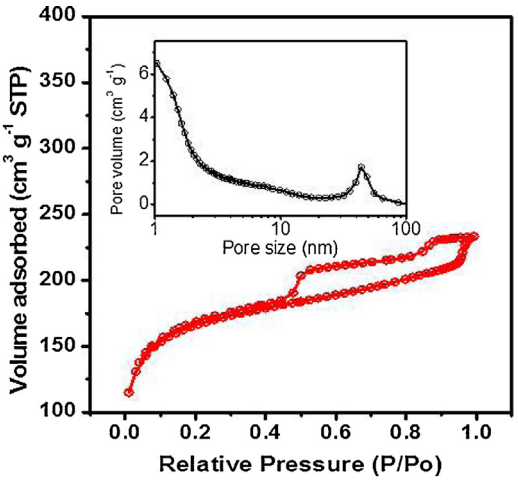

Fig. 4. Nitrogen isothermal adsorption/desorption curves of 3D Fe-N-C catalyst. Inset in Fig. 4 is its pore size distribution.

microstructural heterogeneity, which in turn restrict their ORR activity [32].

Ordered porous carbon frameworks with an interconnecting mesoporous structure not only can provide multidimensional electron transport pathways and short diffusion channels for the penetration and transportation of species, but also can offer large number of active sites for catalytic reaction due to the increased surface area [33,34]. Such these features make them very promising in electrochemical devices for energy conversion and storage. On the other hand, Ferroporphyrin is a red complex of porphyrin and iron in which iron and nitrogen are well-distributed [35]. In the present work, for first time is presented a new three-dimensional (3D) iron-embedded nitrogen doped carbon (3D Fe-N-C) framework, with ordered mesoporous structure as high-efficient and stable ORR catalyst for MFCs based on Ferroporphyrin. As it will be seen below, the 3D Fe-N-C frameworks obtained by pyrolysis of Ferroporphyrin with a silica sphere template possess unique structural advantages of well-ordered mesopores, high surface area ($584\,m^2\,g^{-1}$), highly conductive 3D interconnected networks as well as well-distributed Fe-N species. As a consequence, the unique carbon-rich skeleton with inherent metal–nitrogen coordination derived 3D Fe-N-C frameworks showed substantially enhanced ORR activity compared to that of commercial Pt/C catalyst in neutral media and alkaline electrolyte. A high-performance MFC device with the as-prepared 3D Fe-N-C as air cathode catalyst and *Escherichia coli* cell as exo-electrogens exhibited a maximum power density of $3118.9\,mW\,m^{-2}$ with excellent durability; was able to steadily operate for more than 250 h.

2. Experimental section

2.1. Preparing the iron-embedded nitrogen doped carbon framework

SiO_2 nanospheres were formed with the aid of a seed growth technique. Typically, to an aqueous solution of L-Arginine (0.1% wt, 150 mL) in a 250 mL conical flask, 10.41 g TEOS was added with vigorously stirring. After refluxed under a stirring speed of 1000 rpm for 24 h, the dispersion was cooled to room temperature naturally and the desired amount of water was added dropwise to form a SiO_2 seed dispersion. The above-synthesized dispersion was then poured into a petri dish and dried at 60 °C. The collected powder was subsequently transferred into a crucible and heated to 550 °C ($1\,°C\,min^{-1}$) with a dwelling time of 6 h in air.

The designed 3D porous Fe-N-C catalysts were synthesized through a solid-state nano-casting method. 1.0 g Ferroporphyrin and 0.25 g SiO_2 nanospheres (template) were physically mixed and subsequently heated in a furnace with the set temperature of 800 °C at a ramp rate of $5\,°C\,min^{-1}$. After kept at that temperature for

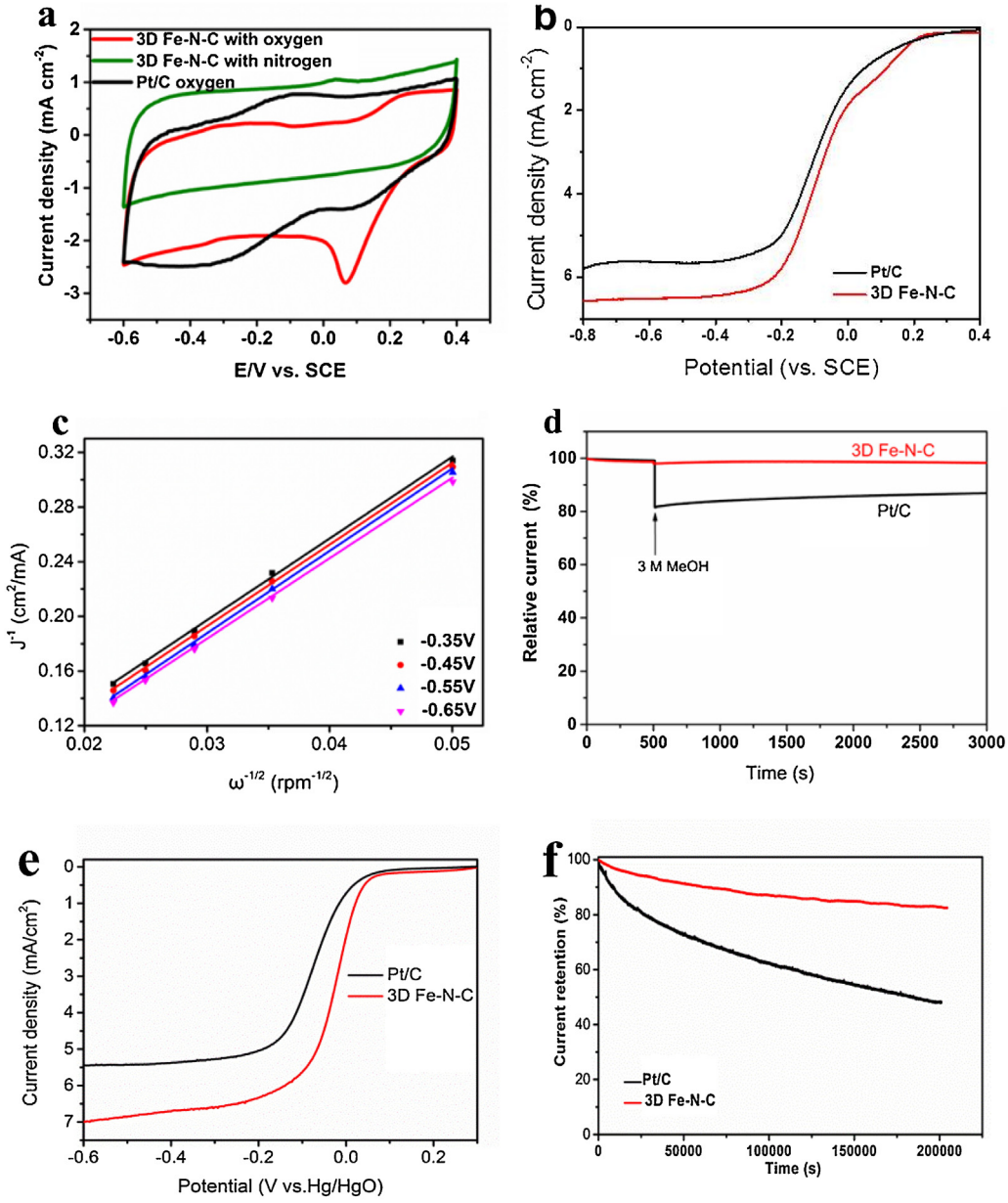

Fig. 5. (a) CV curves of 3D Fe-N-C and Pt/C electrodes in O_2 and Ar saturated 0.01 M PBS solution. (b) LSV curves of the 3D Fe-N-C and Pt/C resulted in O_2-saturated 0.01 M PBS at 10 mV s^{-1} at 1600 rpm. (c) K-L plots of current density versus$\omega^{-1/2}$ at different potentials on 3D Fe-N-C electrode. (d) Current retention curves of the 3D Fe-N-C and Pt/C electrodes with the injection of methanol. (e) LSV curves of the Pt/C and 3D Fe-N-C electrodes collected in O_2–saturated 0.1 M KOH. (f) Current retention curves of the 3D Fe-N-C and Pt/C electrodes recorded at −0.3 V in O_2-saturated 10 mM PBS electrolyte for 55.5 h with a rotation speed of 1600 rpm.

3 h, the samples were cooled down to room temperature under Ar flow. The received powders were placed into HF (10 wt%) aqueous solution for 24 h to remove the nano-silica template. The resulting products were collected by centrifugation, repeatedly washed with DI water, and finally dried at 80 °C.

2.2. Material characterization

The morphology of synthesized materials was investigated using a Zeiss Ultra Plusfeild emission scanning electron microscope (FE-SEM, Ultra Plus-43-13). High resolution TEM and energy dispersive X-ray spectroscopy (EDS) for elemental mapping were carried out on a JEOL JEM 2010F with an acceleration voltage of 200 kV. X-ray photoelectron spectroscopy (XPS) was recorded from a PHI 5000 Versa Probe ULVAC instrument. Nitrogen adsorption-desorption measurements were performed at 77 K in a N_2 atmosphere after degassing the samples at 150 °C under vacuum for 10 h, using a Quantachrome-Quadrasorb SI porosimeter. For calculation of apparent surface area, Brunauer-Emmett-Teller (BET) model was applied to the isotherm data points of the adsorption segment in the relative pressure range $P/P_0 > 0.9$. The pore size distribution was calculated from nitrogen adsorption-desorption plots using the nonlocal density functional theory (NLDFT) equilibrium model method for slit pores provided by supplier.

2.3. Electrochemical characterization

The thin film electrodes were fabricated by drop-coating a catalyst ink on a mirror-polished glassy carbon (GC) electrode with an area of 0.196 cm^2. To prepare the catalyst inks, a suspension consisting of 3D Fe-N-C or Pt/C (5 mg), Nafion® solution (5 wt%, 20 μL), DI water (100 μL) and isopropyl alcohol (900 μL) were ultrason-

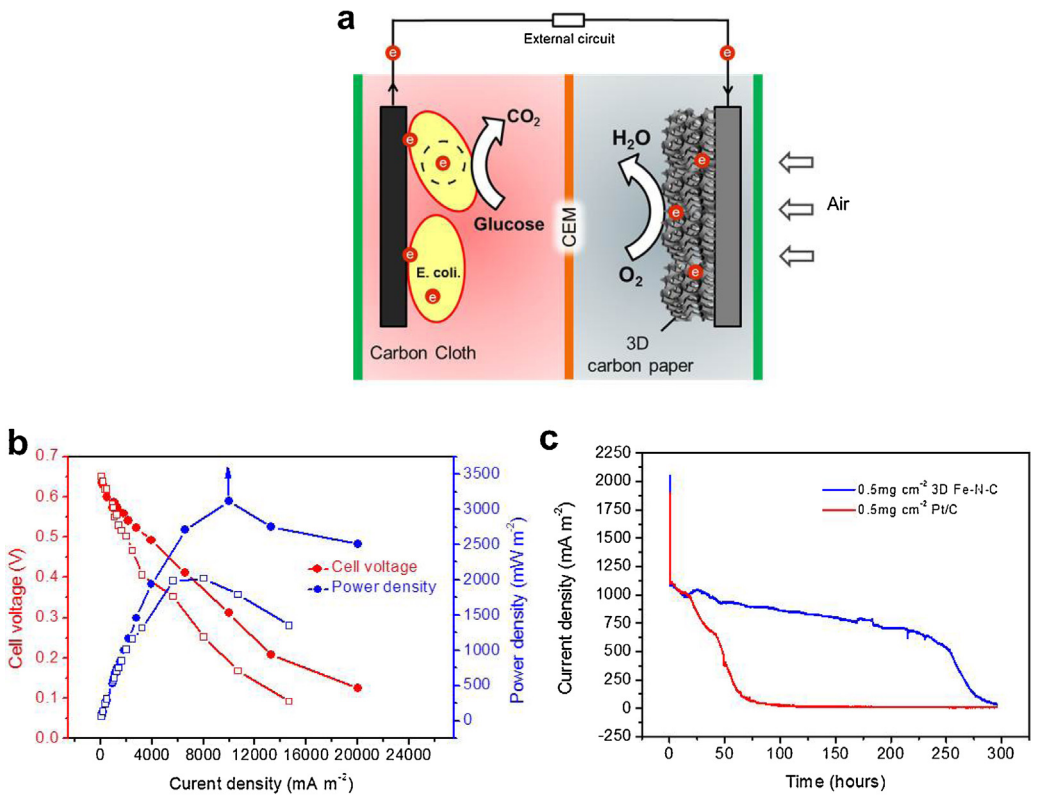

Fig. 6. (a) Schematic diagram of the configuration for the as-fabricated MFC device with carbon cloth anode and 3D Fe-N-C catalyst loaded carbon paper cathode. (b) Comparison of polarization curves and power outputs for the Pt/C-MFC and Fe-N-C-MFC devices. (c) Power output of the Fe-N-C-MFC device as a function of operating time with an external load resistance of 500 Ω.

icated for 30 min. After pipetted 20 μL of catalyst ink on the GC electrode, the thin film electrodes was thus formed by drying at 60 °C.

To evaluate the electrochemical catalytic activity, the as prepared working electrodes were immersed into electrolyte solution of 0.1 M KOH aqueous solution or 0.01 M PBS (10.00 g L^{-1} of $NaHCO_3$ and 11.20 g L^{-1} of $NaH_2PO_4{\cdot}2H_2O$, pH = 7.0) buffer solution. The measurements were performed using a saturated *Calomel electrode* (SCE) as reference electrode and a *Platinum black* as counter electrode in a three-electrode configuration. CV measurements were performed from 0.4 to −0.6 V with a scanning velocity of 50 mV s^{-1}, in both Ar-saturated and O_2-saturated electrolytes. The oxygen reduction currents were determined by cathodically scanning the working electrode between 0.2 and −0.6 V with 5 mV s^{-1} in O_2-saturated electrolytes. The cathodic scan obtained from RDE measurements was corrected according capacitive currents under cathodic scans at 5 mV s^{-1} in Ar-saturated electrolyte.

The fuel cell performance was tested in an air-cathode single-chamber MFC [36]. The assembled MFC consists of carbon cloth (AvCarb 1071 HCB, Fuel Cell Earth) as anode, cation exchange membrane electrolyte, and catalysts (3D porous Fe-N-C catalysts or 40 wt% Pt/C) pasted carbon paper as air cathodes. The mass loading of catalysts was ~0.5 mg cm^{-2}, while the effective area of the air cathode was 4 cm × 4 cm. For the MFC experiments, 2 mL of an overnight *E. coli* K-12 culture was inoculated to 18 mL anolyte (PBS solution with 5×10^{-3} M 2-hydroxy-1,4-naphthoquinone, 10 g L^{-1} glucose, 5 g L^{-1} yeast extract). The polarization curves and power outputs were recorded after inoculation for 6 h.

3. Results and discussion

3D porous Fe-N-C catalysts were synthesized via a solid-state nanocasting method. The whole synthesis process is illustrated in Fig. 1a. Ordered packed silica spheres with a diameter of 40 nm were selected as the scaffold template for 3D ordered porous structure (Fig. 1a).

Ferroporphyrin was employed as the carbon, iron and nitrogen source and was mixed with silica spheres. After ground for 10 min in a mortar, a blue mixture was obtained. Then, the mixture was carbonized at 800 °C for 3 h in Ar atmosphere to form ordered Fe-N-C/silica. Finally, black 3D porous Fe-N-C powder was successfully prepared after removing the silica spheres in a HF aqueous solution.

Scanning electron microscopy (SEM) images reveal that a 3D well-interconnected network with mesoporous walls (Fig. 1c) was obtained, whose diameter is similar to that of the used silica spheres (Fig. 1b), indicating the successful inverse replication of the silica template. The detailed microstructure of the 3D Fe-N-C catalyst was further studied by transmission electron microscopy (TEM). Fig. 2a shows a typical TEM micrograph of the 3D Fe-N-C catalyst, exhibiting a well-defined mesoporous structure of the 3D Fe-N-C sample. Moreover, Fe nanoparticles were uniformly embedded in the matrix of 3D porous structure (labelled by white arrows in Fig. 2a).

Fig. 2b presents the high-resolution TEM (HRTEM) image obtained for the 3D Fe-N-C sample, which confirms that the Fe nanoparticles were entirely encapsulated within graphitic carbon nanoshells. The well-resolved lattice fringes of 0.19 nm corresponding to the (002) planes of iron (Joint Committee on Powder Diffraction Standards #50–1275) are clearly observed, demonstrating that the Fe nanoparticles are highly crystalline in nature.

Electron energy loss spectroscopy (EELS) elemental mappings were acquired to reveal the presence of carbon, nitrogen and iron in the Fe-N-C catalyst (Fig. 2c–f). As it can be seen, the C, N, and O elements were homogeneously distributed throughout the 3D matrix of the Fe-N-C sample. Unexpectedly, apart from the intensive Fe signals from the iron particles, Fe species were also detected

on other sections. Such finely dispersive Fe species could possibly bond with the neighbouring C or N atoms, which are believed to be highly active for ORR [26].

X-ray photoelectron spectroscopy (XPS) analysis was performed to determine the chemical composition of the as-prepared Fe-N-C catalyst. From the XPS survey scan spectrum (Fig. 3a), only Fe, C, N, and O singles were detected, showing the high purity of the Fe-N-C catalyst. As it can be seen from Fig. 3b, the core level C 1s XPS peak deconvolution reveals the presence of four types of C functionalities in Fe-N-C catalyst, which correspond to C=C (284.6 eV), C—O (285.3 eV), C=O (286.5 eV) and C—N (288.2 eV) bonds, respectively [37–39].

Fig. 3c shows the core level N 1s XPS spectrum, which can be deconvoluted into three peaks. The peaks centered at 398.4, 400.1, and 401.1 eV are assigned to pyridinic N, pyrrolic N, and graphitic N, respectively [37,38]. In addition, due to the small difference on the binding energy between graphitic N and Fe-N, the peak at 401.1 eV may also include a contribution from Fe bound to N (Fe-N) [28,29]. The graphitic-N and Fe-N could serve as ORR catalytic sites, as reported both experimentally and theoretically, and thus can greatly increase the ORR activity. These results further demonstrate that Fe and N heteroatoms have been doped into the 3D carbon framework.

The surface area and pore size of the Fe-N-C catalyst were determined by N_2 adsorption/desorption isothermal analysis. The Brunauer-Emmett-Teller (BET) surface area for the Fe-N-C catalyst is calculated to be 584 $m^2 g^{-1}$, with a total pore volume of 0.36 $cm^3 g^{-1}$. As shown in Fig. 4, the Fe-N-C catalyst exhibited Type-IV isotherm (as defined by IUPAC), characteristic sorption behaviour of mesoporous materials. The adsorption branch of the isotherm give a sharp capillary condensation step occurred in the region of $P/P_0 > 0.9$, indicative of the presence of numerous mesopores. As expected, the pore size distribution (PSD) curve estimated from adsorption data using the Barrett-Joyner-Halenda (BJH) model gives an average pore size of about 42 nm. The value is slightly larger than the size of the primary silica spheres.

To evaluate the ORR activity of the as-prepared 3D Fe-N-C catalyst, the cyclic voltammetry (CV) measurements were firstly conducted in a neutral pH solution, which is commonly employed as the electrolyte in biological systems. For comparison reasons, a commercial Pt catalyst (20 wt% Pt/C) was also tested under the same conditions.

Fig. 5a shows the CV curves of the Pt/C and 3D Fe-N-C electrodes recorded at 10 mV s^{-1} in a solution of Ar and O_2-saturated 10 mM PBS (pH 7.0). As it can be seen, a distinct ORR peak centered at ca. −0.08 V (vs. SCE) is observed in presence of oxygen for 3D Fe-N-C electrode, while in absence of oxygen no ORR peak is observed, showing that the as-prepared 3D Fe-N-C electrode exhibits good ORR activity. Additionally, the similarity of the comparison of the CV curves of Pt/C and 3D Fe-N-C electrodes also reveals that 3D Fe-N-C possesses an outstanding ORR electrocatalytic activity in neutral PBS solution. To qualify the ORR process on the 3D Fe-N-C catalyst, linear sweep voltammogram (LSV) curves of Pt/C and 3D Fe-N-MC catalysts were recorded by the aid of a rotating disc electrode (RDE) (Fig. 5b). Remarkably, the 3D Fe-N-C electrode showed a more positive ORR onset potential (0.23 V vs. SCE) and half-wave potential (−0.08 V vs. SCE) than those of the commercial Pt/C electrode. These present onset and half-wave potentials are also significantly more positive than the values of recently reported non-noble-based catalysts in neutral electrolyte [30,40–46], such as N doped graphene [41], N doped carbon nanofibers [40], Fe/N doped carbon [42], N-Fe/Fe_3C@C [30], and N-P co-doped porous carbon foams [43]. Furthermore, the 3D Fe–N—C electrode afforded an extremely stable diffusion-limiting current of ~6.2 mA cm^{-2}, which is also superior to that observed on Pt/C electrode (~5.3 mA cm^{-2}) and on most of recently investigated ORR catalysts in neutral electrolyte. LSV curves of 3D Fe-N-C electrode in 0.1 M KOH electrolyte were shown in Fig. 5e, 3D Fe-N-C catalyst exhibited more positive onset potential and higher diffusion-limiting current than that of benchmark Pt/C catalyst. These results unambiguously demonstrate that the as-prepared 3D Fe-N-C sample has an ultrahigh ORR catalytic activity in neutral and alkaline electrolyte.

For further insight into the ORR kinetics of the 3D Fe-N-C catalyst, the electron-transfer numbers (n) of the samples were analysed on the basis of the Koutecky–Levich (K–L) equation [43]. Fig. 5c shows the K-L plots obtained by linear fitting of the inverse square root of rotating speed vs. reciprocal current density at rotation rate from 400 to 2000 rpm. The linear K-L plots suggest that the 3D Fe-N-C acts up to the first-order reaction kinetics toward the concentration of O_2 from −0.35 to −0.65 V. The electron transfer numbers (n) for 3D Fe-N-C were calculated from the slopes of K-L plots to be 3.83–4.03 at potentials ranging from −0.35 to −0.65 V, which are comparable to those of commercial Pt/C catalyst. This clearly reveals a four-electron process toward ORR on the 3D Fe-N-C electrode.

To demonstrate that the as-prepared 3D Fe-N-C catalyst is a promising candidate for MFCs, its long-term durability has also been evaluated by chronoamperometry measurements at −0.3 V (vs. SCE) for 55.5 h in O_2-saturated 10 mM neutral PBS. As shown in Fig. 5f, the 3D Fe-N-C catalyst exhibits substantially higher stability than commercial Pt/C with more than 82.4% retention of its initial electrochemical activity after 55.5 h. The observed stability is also considerably better or at least comparable to the recently reported catalysts [30,40–45]. Furthermore, the 3D Fe-N-C catalyst shows a significantly better tolerance to methanol crossover than commercial Pt/C (Fig. 5d), indicating that the as-obtained 3D Fe-N-C catalyst holds great potential as ultra-stable ORR catalyst. The substantially superior ORR activity of the 3D Fe-N-C can be attributed to its unique structural features: (1) the finely dispersive Fe and N species as well as high surface area (~584 $m^2 g^{-1}$) afford a full exposure for active sites that ensure them can interact closely O_2; (2) the ordered mesoporous structure can provide short diffusion channels for the penetration and transportation of O_2 and ions, and thus enable fast mass exchanges during the ORR process; and (3) the interconnected 3D carbon frameworks networks with high conductivity can effectively facilitate electron transfer.

To test feasibility of the as-obtained 3D Fe-N-C as a cathodic ORR catalyst for MFCs, an air-cathode single-chamber MFC device was fabricated by using 3D Fe-N-C as ORR catalyst (cathode) as previously described (denoted as Fe-N-C-MFC, see Experimental section).

Fig. 6a displays the configuration of the as-fabricated MFC device, which consists of a commercial carbon cloth (AvCarb 1071 HCB, FuelCellEarth) as anode, a cation exchange membrane (CEM), and a 3D Fe-N-C loaded carbon paper (0.5 mg cm^{-2}) as cathode directly exposed to the air. In the anode chamber, Escherichia coli. (*E.coli.*) cell was used to generate electrons from the organic substrate. It should be noted that it is difficult to compare the MFC performance directly with literature results, due to the different adopted parameters, since the performance of MFC can be influenced by many factors, such like cathodic reaction, buffer system, inoculated bacterial strain, cell configuration, organic substrate and et al. In order to illustrate the advantage of our 3D Fe-N-C sample catalyst, an another similar MFC device with a 40 wt% Pt/C loaded carbon paper (0.5 mg cm^{-2}, a common cathode catalyst for MFCs) as anode (denoted as Pt/C-MFC) was set as control. In Fig. 6b, the polarization curves and power outputs of the as-fabricated Pt/C-MFC and Fe-N-C-MFC are compared. Notably, the open-circuit potential of the Fe-N-C-MFC is ca. 0.63 V; almost the same with that of Pt/C-MFC (0.65 V). However, with the decreasing load resistance, the cell voltage of the Fe-N-C-MFC device decreased more slowly

compared to the Pt/C-MFC device, suggesting the superior ORR activity and charge transfer rate of the Fe-N-C-MFC device. More importantly, the Fe-N-C-MFC could deliver a maximum power density of 3118.9 mW m^{-2} (based on the projected surface area of the anode, details see Experimental section), which is dramatically higher than the value obtained for Pt/C-MFC (2017.6 mW m^{-2}) at the same operated conditions. Moreover, the Fe-N-C-MFC has an excellent long-term durability. As shown in Fig. 6c, with a 500 Ω external resistor, the output power density of the Fe-N-C-MFC is substantially larger than that of Pt/C-MFC all the time during the whole operating period, in which the *E.coli* density in the anodic chamber remained unchanged. Additionally, the Fe-N-C-MFC was able to steadily operate for more than 250 h, while only less than 50 h for the Pt/C-MFC. Such the inferior durability of the Pt/C-MFC is believed to due to the deterioration of electrocatalytic activity of the Pt/C cathode catalyst. All these results certainly highlight that the as-synthesized 3D Fe-N-C catalyst had superb electrocatalytic activity and stability for ORR and holds great potential as a promising catalyst in MFCs with a long operation time.

4. Conclusions

In summary, a 3D Fe-embedded N doped carbon framework catalyst with outstanding ORR performance in a neutral pH solution has been successfully developed and tested as a robust cathode catalyst for MFCs. Due to the well-arranged mesopores, high surface area, interconnected conductive networks as well as finely dispersed Fe-N active species, the as-prepared 3D Fe-N-C catalyst exhibits significantly enhanced ORR activity as compared to commercial Pt/C catalyst. The 3D Fe-N-C yields a more-positive half-wave potential of −0.08 V (vs. SCE) and remarkably stable limiting current of ~6.2 mA cm^{-2} in a neutral PBS electrolyte. Additionally, the 3D Fe-N-C also has an excellent tolerance to methanol as well as remarkably long-term stability with more than 82.4% retention of its initial activity after 55.5 h. Moreover, a stable MFC device with high power density output was fabricated based on the as-prepared 3D Fe-N-C as cathode (air) catalyst. The as-fabricated Fe-N-C MFC device is able to deliver a maximum power density of 3118.9 mW m^{-2} at a high current density of 9980.8 mA m^{-2}. More importantly, the Fe-N-C MFC device could steadily operate for more than 250 h in a feed period, which is substantially longer than the Pt/C-MFC device. The capability of using low cost metal and nitrogen doped carbon framework materials with unique structural features and well-distributed active species not only is crucial for the large-scale application of MFCs, but also opens up new opportunities to nanostructured carbon materials for fuel cells, batteries, supercapacitors, etc.

Acknowledgements

We acknowledge the National Natural Science Foundation of China (51472187, 51272200, 61376064), Program for New Century Excellent Talents in University (NCET-12-0911) and Guangdong Natural Science Foundation for Distinguished Young Scholar (2014A030306048) for financial support.

Prof. Tsiakaras is also grateful to the "Bilateral R&D Co-operation between Greece and China 2012-2015" and to the Ministry of Education and Science of the Russian Federation (Mega-grant contract No. 14.Z50.31.0001), for financial support.

References

[1] S.K. Chaudhuri, D.R. Lovley, Nat. Biotechnol. 21 (2003) 1229–1232.
[2] J.E. Mink, R.M. Qaisi, B.E. Logan, M.M. Hussain, NPG Asia Mater. 6 (2014) e89.
[3] C.H. Kwon, S.-H. Lee, Y.-B. Choi, J.A. Lee, S.H. Kim, H.-H. Kim, G.M. Spinks, G.G. Wallace, M.D. Lima, M.E. Kozlov, Nat. Commun. 5 (2014).
[4] U. Schröder, J. Nießen, F. Scholz, Angew. Chem. Int. Ed. 42 (2003) 2880–2883.
[5] R. Allen, H.P. Bennetto, Appl. Biochem. Biotechnol. 39–40 (1993) 27–40.
[6] Y.-P. Xiao, W.-J. Jiang, S. Wan, X. Zhang, J.-S. Hu, Z.-D. Wei, L.-J. Wan, J. Mater. Chem. A 1 (2013) 7463–7468.
[7] M.K. Debe, Nature 486 (2012) 43–51.
[8] R. Devivaraprasad, R. Ramesh, N. Naresh, T. Kar, R.K. Singh, M. Neergat, Langmuir 30 (2014) 8995–9006.
[9] Y. Chang, F. Hong, C. He, Q. Zhang, J. Liu, Adv. Mater. 25 (2013) 4794–4799.
[10] H. Yu, Y. Li, X. Li, L. Fan, S. Yang, J. Chem. Eur. 20 (2014) 3457–3462.
[11] J.B. Wu, H. Yang, Acc. Chem. Res. 46 (2013) 1848–1857.
[12] Z. Wang, S. Xiao, Z. Zhu, X. Long, X. Zheng, X. Lu, S. Yang, ACS Appl. Mater. Interfaces 7 (2015) 4048–4055.
[13] L. Xu, Q. Jiang, Z. Xiao, X. Li, J. Huo, S. Wang, L. Dai, Angew. Chem. Int. Ed. 55 (2016) 5277–5281.
[14] A. Brouzgou, S.Q. Song, P. Tsiakaras, Appl. Catal. B: Environ. 127 (2012) 371–388.
[15] J. Jin, F. Pan, L. Jiang, X. Fu, A. Liang, Z. Wei, J. Zhang, G. Sun, ACS Nano 8 (2014) 3313–3321.
[16] S. Chen, J. Duan, M. Jaroniec, S.Z. Qiao, Adv. Mater. 26 (2014) 2925–2930.
[17] J.W. Xiao, G.L. Xu, S.G. Sun, S.H. Yang, Part. Part. Syst. Charact. 30 (2013) 893–904.
[18] K. Wan, G.-F. Long, M.-Y. Liu, L. Du, Z.-X. Liang, P. Tsiakaras, Appl. Catal. B: Environ. 165 (2015) 566–571.
[19] X. Chen, X.H. Chen, X. Xu, Z. Yang, Z. Liu, L.J. Zhang, X.J. Xu, Y. Chen, S.M. Huang, Nanoscale 6 (2014) 13740–13747.
[20] J. Liang, Y. Jiao, M. Jaroniec, S.Z. Qiao, Angew. Chem. Int. Ed. 51 (2012) 11496–11500.
[21] S.A. Wohlgemuth, R.J. White, M.G. Willinger, M.M. Titirici, M. Antonietti, Green Chem. 14 (2012) 1515–1523.
[22] Y. Hua, T. Jiang, K. Wang, M. Wu, S. Song, Y. Wang, P. Tsiakaras, Appl. Catal. B: Environ. 194 (2016) 202–208.
[23] T. Jiang, Y. Wang, K. Wang, Y. Liang, D. Wu, P. Tsiakaras, S. Song, Appl. Catal. B: Environ. 189 (2016) 1–11.
[24] D.-S. Yang, D. Bhattacharjya, S. Inamdar, J. Park, J.-S. Yu, J. Am. Chem. Soc. 134 (2012) 16127–16130.
[25] C. Zhang, N. Mahmood, H. Yin, F. Liu, Y. Hou, Adv. Mater. 25 (2013) 4932–4937.
[26] X. Zhou, Z. Bai, M. Wu, J. Qiao, Z. Chen, J. Mater. Chem. A 3 (2015) 3343–3350.
[27] Q. Liu, J. Zhang, Langmuir 29 (2013) 3821–3828.
[28] G. Wu, C.M. Johnston, N.H. Mack, K. Artyushkova, M. Ferrandon, M. Nelson, J.S. Lezama-Pacheco, S.D. Conradson, K.L. More, D.J. Myers, P. Zelenay, J. Mater. Chem. 21 (2011) 11392–11405.
[29] H.-W. Liang, W. Wei, Z.-S. Wu, X. Feng, K. Müllen, J. Am. Chem. Soc. 135 (2013) 16002–16005.
[30] Z. Wen, S. Ci, F. Zhang, X. Feng, S. Cui, S. Mao, S. Luo, Z. He, J. Chen, Adv. Mater. 24 (2012) 1399–1404.
[31] D. Chen, H. Feng, J. Li, Chem. Rev. 112 (2012) 6027–6053.
[32] L. Lin, Q. Zhu, A.W. Xu, J. Am. Chem. Soc. 136 (2014) 11027–11033.
[33] S. Lu, D. Wang, S.P. Jiang, Y. Xiang, J. Lu, J. Zeng, Adv. Mater. 22 (2010) 971–976.
[34] Y. Zhou, J. Yang, H. Su, J. Zeng, S.P. Jiang, W.A. Goddard, J. Am. Chem. Soc. 136 (2014) 4954–4964.
[35] M.A. Stanford, J.C. Swartz, T.E. Phillips, B.M. Hoffman, J. Am. Chem. Soc. 102 (1980) 4492–4499.
[36] H. Tang, S. Cai, S. Xie, Z. Wang, Y. Tong, M. Pan, X. Lu, Adv. Sci. 3 (2016) 1500265.
[37] S.-A. Wohlgemuth, T.-P. Fellinger, P. Jaker, M. Antonietti, J. Mater. Chem. A 1 (2013) 4002–4009.
[38] C.H. Choi, S.H. Park, S.I. Woo, Green Chem. 13 (2011) 406–412.
[39] Y. Wang, Y. Liu, K. Wang, S. Song, P. Tsiakaras, H. Liu, Appl. Catal. B: Environ. 165 (2015) 360–368.
[40] X. Yang, W. Zou, Y. Su, Y. Zhu, H. Jiang, J. Shen, C. Li, J. Power Sources 266 (2014) 36–42.
[41] L. Feng, Y. Chen, L. Chen, ACS Nano 5 (2011) 9611–9618.
[42] L. Birry, P. Mehta, F. Jaouen, J.-P. Dodelet, S. Guiot, B. Tartakovsky, Electrochim. Acta 56 (2011) 1505–1511.
[43] H. Jiang, Y. Zhu, Q. Feng, Y. Su, X. Yang, C. Li, Chem. Eur. J. 20 (2014) 3106–3112.
[44] M. Seredych, J.-C. Idrobo, T.J. Bandosz, J. Mater. Chem. A 1 (2013) 7059–7067.
[45] Y. Su, H. Jiang, Y. Zhu, W. Zou, X. Yang, J. Chen, C. Li, J. Power Sources 265 (2014) 246–253.
[46] Z. Guo, Y. Qiao, H. Liu, C. Ding, Y. Zhu, M. Wan, L. Jiang, J. Mater. Chem. 22 (2012) 17153–17158.